DOI: 10.13009/EUCASS2019-938

Numerical simulation of three-dimensional cylinder flare at hypersonic flows

Amjad A. Pasha[1], M. Khalid[2] and K. A. Juhany[3]*
[1]Assistant Professor, [2]Professor, [3]Chairman
Department of Aeronautical Engineering, King Abdulaziz University, Jeddah- 21589, Saudi Arabia.
**Corresponding author email: aapasha@kau.edu.sa*

Abstract

Shock boundary layer interaction provoked from corners and junctions on missile bodies with flare geometry, or between missiles bodies and lifting surfaces and/or control surface mechanism may lead to unsteady loads and other heating problems. The steady-state Navier-Stokes algorithms typically used to understand such aerodynamic and thermodynamic performance may average out such unsteady transients aggravating the problem. The unsteadiness in the junction region, where the shock emanating from the corner and growing boundary layer from the straight portion of the configuration try to co-adjust with the flow leading to a bubble which strides across the junction. The flow in this bubble is strongly reversing leading to a local separation and reattachment later the inclined surface. A Navier-Stokes code typically used for steady calculations will try to force steadiness upon an otherwise unsteady flow in the junction region and continue to face numerical unsteadiness in this region leading to oscillatory behavior which impedes the progress towards required convergence. Reynolds-averaged Navier-Stokes simulations are performed on the two-dimensional and three-dimensional large hollow cylinder flare configuration of the same model at a Mach of 5 and a unit Reynolds number of 1.2 x 107. Both standard and production limiter version of k-ω turbulence model is employed in the simulations. The variations of grid size on the flow gradients such as shock waves and boundary layer are studied in detail to establish the grid independent solution.

1. Introduction

Shock wave/boundary layer interactions (SBLI), especially in the junction region, have strong implications in hypersonic flows. The shock waves generated from the boosters of launch vehicle interacts with the boundary layer from the front cylindrical portion of the vehicle to form distinct SBLI regions fraught with separated reversing flows which interfere with the prevailing shock patterns. Invariably, the boundary layer separates as a result of this interference and produces unsteadiness in the flow before reattachment on the aft inclined surface. The presence of strong shock in the junction region and the interplay between the separated bubble which astride the junction, produces accentuated aerothermodynamic loads near the rear of the separation region. The SBLI on the exterior surface of the launch vehicle can cause loss of control due to aerothermodynamic loading. Therefore, the design of the thermal protection system for hypersonic vehicles needs an accurate prediction of surface wall pressure and heat flux and detail understanding of SBLI flows.

The presence of unsteadiness in the flow coupled with strong separation and reversing flows renders most one and two-equation models incapable of predicting flows accurately. Thus, it is a difficult task to use Reynolds-averaged Navier-Stokes equations (RANS) with available two-equation turbulence models to compute the flows accurately. It is a challenging task, especially to predict the peak wall pressure and associated heat flux. Most of the computed studies thus far have been limited to equivalent two-dimensional axisymmetric flows [1].

RANS based algorithms have been used quite frequently with appropriate modifications to standard turbulence models in order to improve SBLI simulations of two-dimensional (2D) and three-dimensional (3D) supersonic and hypersonic studies [2],[3],[4][5],[6],[7]. Knight and Degrez [3] observed that the hypersonic flow at Mach 5 past axisymmetric cylinder flare configuration containing shock boundary layer interaction differs from the corresponding flow past 2D geometry. It is noted that in the latter case that it leads to a weaker shock angle for the same deflection angle. The existence of non-uniformity of the flow downstream of a conical shock was hardly noticeable for the cases they considered. Whereas, the skin friction was observed to be non-zero in the 3D STBLI regions in single and double fin configurations.

DOI: 10.13009/EUCASS2019-938

Huang and Coakley [39] used compressibility corrections in SWTBLI compression corner flows to improve heat flux in the interaction region. Wilcox [42] computed with his modified k-ω turbulence model with stress limiter hypersonic turbulent SWTBLI at Mach 11 for the axisymmetric body. The initial pressure location and wall pressure distribution were better predicted with the stress limiter k-ω turbulence model in comparison to its standard form of the turbulence model. He recommends not to use compressibility modifications in the turbulence model as they deteriorate solution in the SWTBLI region. The heat flux is predicted 50% higher in the reattachment region in comparison to the experiments by both versions of the turbulence model. Zhang et al. [24] improved the heat flux in the shock/boundary layer interaction region over axisymmetric cone-cylinder-flare body at Mach 7 using modified k-ω SST turbulence model. The modification involved an adjustment to the production limiter which eliminated the nonphysical increase of the turbulent quantities across a shock wave and therefore enhanced the accuracy of the aerothermal prediction in the SBLI region especially the reattachment region. Gnoffo[8] simulated the flow past axisymmetric geometries, namely two hollow cylinders with sharp leading edges and 30° flares and a sharp double cone (25°/55°). The geometries were approximately 20 cm in length and 13 to 26 cm in diameter. The flow conditions varied between Mach 9.5 to 11.4 and Reynolds numbers from $1.44x10^5$ to $3.6x10^5$ per meter. The computations showed the increasing extent of separation bubble with increasing Reynolds number and significant shifting of the separation region over the range. The Mach number did not show a significant effect on the separation region for the range of flow conditions considered. All simulations required finer grids of dimension 1512x192 in order to achieve grid converged results. The sharp double cone results at the lowest Reynolds number appeared to show grid convergence with a mesh having 1024x256 grid points, but massive instabilities were observed with additional grid points. Candler [9] observed that the separation bubble size increases as the grid are doubled in each direction for hypersonic laminar flows over the double cone and for the cylinder flare configurations. The mesh refinement study was systematically conducted, and the computations were carried out to see its effect on solutions. The mesh refinement study did not involve just increasing the grid density in the normal or axial direction without due consideration to specific physics. It was imperative to make the mesh geometrically increase in density in the separation region and downstream in the vicinity of the junction region and where the peak loads are likely to occur. Towards this end, several meshes were run to capture accuracy. It was observed that the size of the separation bubble is a strong function of the grid refinement. The solution seems to converge for a mesh of dimension 1024 x 512. Nompelis et al. [10] computed laminar hypersonic flow over 2D and 3D double cone cylinder flare configurations. A baseline grid of 512×256 points is used, which was subsequently refined to 1024×512 points with y+ values well below 1. The refined grid was observed to give a slightly larger separation zone.

Turbulent flows which dominate the physics in the junction region are three-dimensional in nature and cannot be captured adequately in a two-dimensional simulation. In the present work, RANS equations coupled with standard k-ω turbulence model are used to solve the two and three-dimensional large hollow cylinder flare configuration at high Mach number. The focus of the work is to study the wall data variations in three-dimensional shock boundary layer interaction regions and compare it with the two-dimensional axisymmetric flows and compare with the experimental data. Also, the variations of grid size on the flow gradients such as shock waves and boundary layer in the streamwise and transverse flow direction are studied in detail to establish the grid independent solution.

The structure of the paper is as follows. The methodology section gives the geometry and flow conditions. This is followed by a section in which the 2D numerical simulation details and results are discussed using a modified Steger Warming method [11] vector flux splitting and data parallel line relaxation (DPLR) method [18]. Next, the 2D and 3D numerical simulation details and results are discussed using the classic Beam and Warming method [12] for implicit approximate factorization of the LHS of the Euler portion of the Navier Stokes equations. Lastly, conclusions and future work are presented.

2. Geometry and flow conditions

Holden [13] performed hypersonic flow experiments over cylinder-flare configuration at varying Mach numbers from 5 to 8, Reynolds number from 1.1 to 6.3×10^7 and wall temperatures from 315 K to 353 K. The large hollow cylinder flare configuration [2] of total length = 2.8 m (109.82 inches) and 36º flare angle is shown in Fig.1. The corresponding flow conditions are shown in Table 1 for one of the test cases. The schlieren images, wall pressure, and heat transfer data were measured in the SBLI region.

DOI: 10.13009/EUCASS2019-938

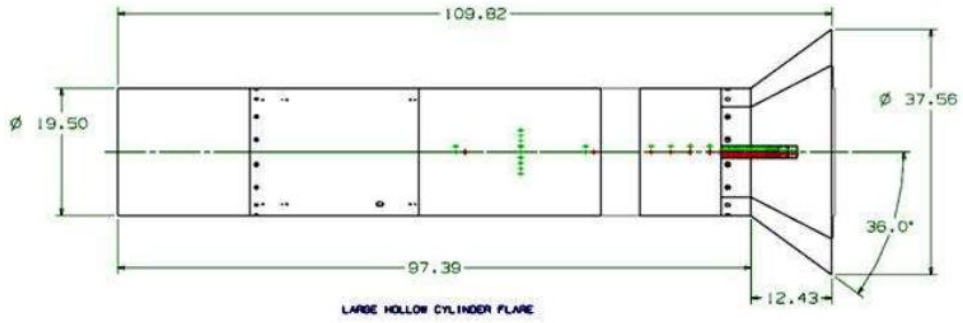

Figure 1: Cylinder flare configuration (dimensions in inches) with 36° flare angle[13].

Table 1. Flow conditions over cylinder-flare configuration.

Flow parameters	Run-17
Freestream Mach number M_∞	4.95
Freestream temperature T_∞, K	213.9
Freestream density ρ_∞ x 10^{-2}, kg m^{-3}	10.93
Freestream pressure P_∞, kPa	6.71
Unit Reynolds number $Re_{1\infty}$, x 10^7, m^{-1}	1.2
Reynolds number based on total length $Re_L x10^7$	3.2
Constant wall temperature, K	315.5
Specific total enthalpy h_0 MJ/kg	1.3

3. Two-dimensional (2D) numerical simulations

Numerical method

The RANS equations for the mean flow, as presented by Wilcox[14] [.] are used in the present simulations. The code of Sinha and Candler [15] is used with standard two-equation k-ω model [16] whereas the Menter et al. modification to k-ω model [17] is also used in the simulations. Both the standard and modified models do not use any compressibility corrections. The RANS equations are fully coupled to turbulence model equations and are discretized using a finite volume formulation. The inviscid fluxes are computed using a modified, low-dissipation form of the Steger-Warming flux splitting approach [11] using a second order both in streamwise and traverse directions. The steady-state solution is reached using the DPLR method of Wright [18].

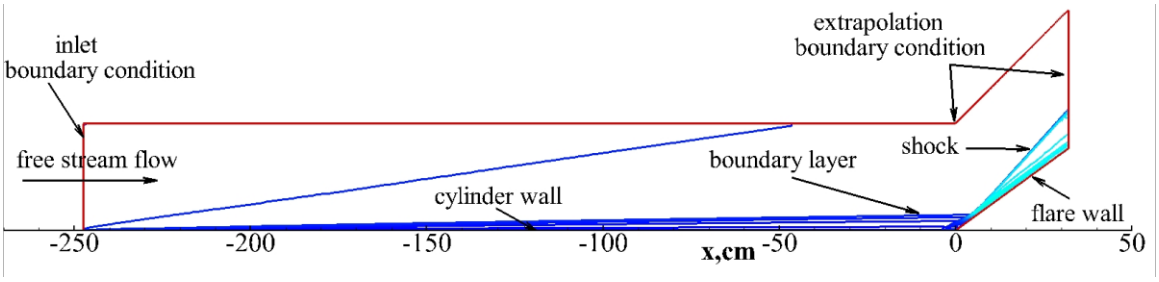

Figure 2: 2D numerical domain with boundary conditions for cylinder flare geometry.

The numerical domain and boundary conditions are identified in Fig. 1. The cylinder-flare corner is taken as origin in the computational domain such that negative values of x are assigned upstream and positive values in the downstream side. A relatively weak shock forms at the sharp leading edge of the cylinder and the strong shock is induced at the location where the flare interacts with the upstream boundary layer formed on the cylinder wall. The grid points are clustered in high gradient flows in the boundary layer near wall region, shock waves, and the separation bubble region at the corner. A structured Cartesian mesh with exponential stretching normal to the wall with the first cell of $1x10^{-6}$ m is used to span the computational domain. This way it is possible to locate more points in the boundary

DOI: 10.13009/EUCASS2019-938

layer region. The grid points are clustered at the cylinder flare junction and are exponentially stretched on both sides with the first cell positioned at $5x10^{-4}$ m from the corner. Following, Menter [19], the free stream conditions for standard and modified k-ω models used for the simulations are $\omega_\infty = U_\infty/L$ and $k_\infty = 0.01\ \nu_\infty\omega_\infty$, where ν is kinematic viscosity, U∞ is the freestream velocity and L = 1 m is a characteristic length. At the cylinder flare, an isothermal cold wall condition corresponding to a temperature ratio of $T_w/T_0 = 0.25$ is maintained with a no-slip condition at the surface and a zero normal pressure gradient applied at the boundary. An extrapolation boundary condition is assigned at top and exit planes For the turbulence quantities, the boundary conditions at the wall [19] are taken as $\mu_{Tw} = 0$, k = 0 and $\omega = 60\nu_w / \beta 1 \backslash \Delta y_1^2$, where β1 = 3/40 and Δy_1 is the normal distance to the grid point nearest to the wall. Based on the grid convergence study, a grid size of dimension 600 x 400 is found to be appropriate for the standard k-ω model as shown in Fig. 3. The wall units of $y^+ < 1$ are obtained in the whole domain. A maximum CFL of 25 is used in the simulations. Hypersonic and supersonic SBLI flows have been validated using this code [20],[21],[22],[23],[24],[25],[26].

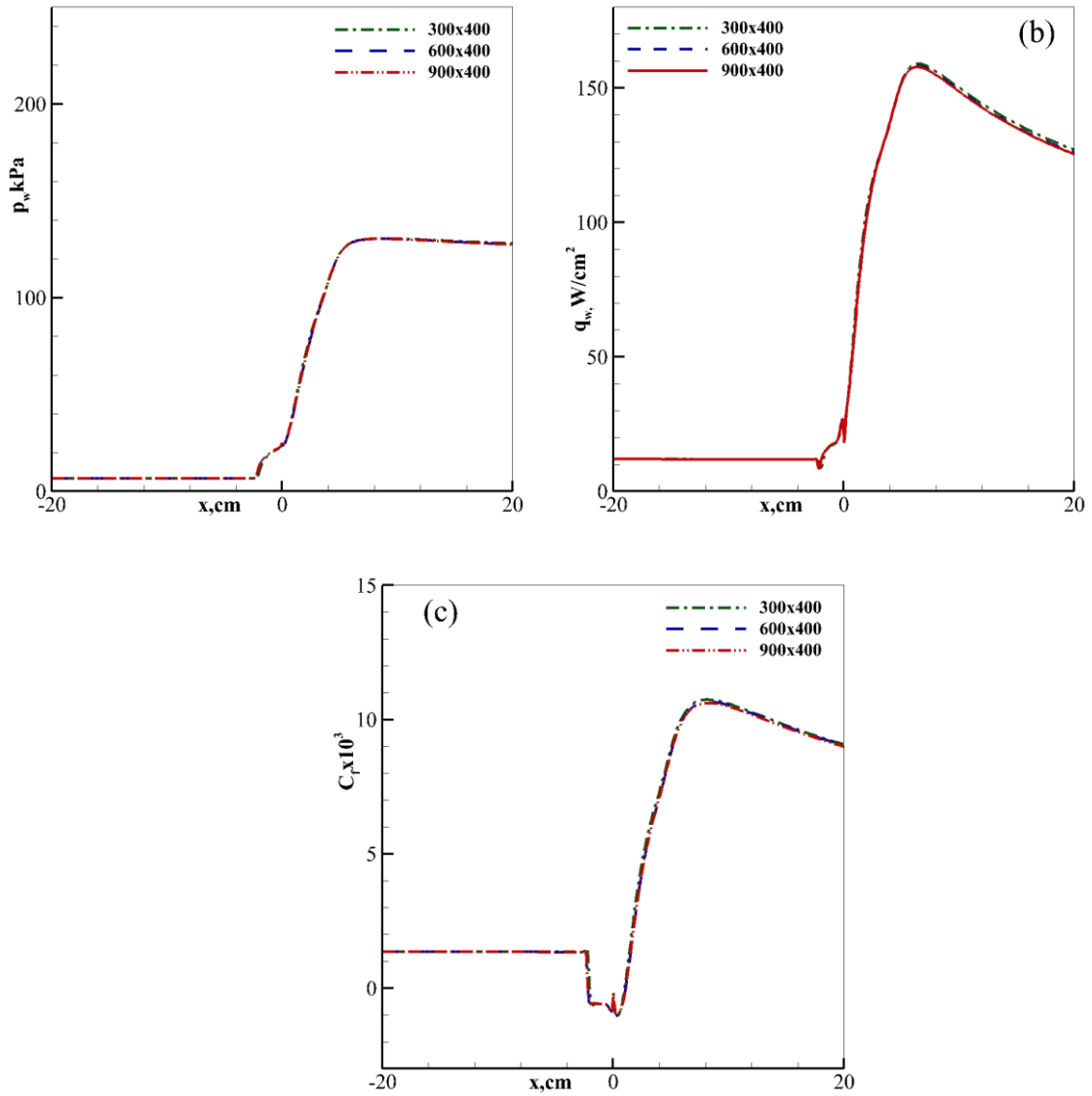

Figure 3: Grid convergence study with varying grid points in the streamwise direction. Computed (a) wall pressure and (b) heat flux and (c) Skin friction using standard two-equation k-ω model [16].

Flowfield and wall data

The computed flow field structure of the hollow cylinder flare interaction is described in detail in Fig. 4. The boundary layer starts thickening before the flare (see Fig.2) and eventually separates at a point S due to the high adverse pressure gradient across shock wave generated at cylinder flare corner. The thickening of the boundary layer generates a series of compression waves which coalesce eventually into a separation shock. The separated shear layer reattaches

DOI: 10.13009/EUCASS2019-938

on the flare to produce a strong reattachment shock. The reattached shock intersects with the separation shock at the triple point T. This shock-shock interaction leads to the formation of an expansion fan and shear layer. The interaction between separation and reattachment shocks generates a transmitted shock, a shear-layer and, depending upon the Mach number, either a shock wave or an expansion fan that interacts with the boundary layer on the flare. This is the reason the separation shock in Fig. 4b is inclined at a higher angle than experimental in Fig. 4c. This impact is shown on the wall pressure in Fig.5a which shows higher plateau than experimental data. The computed triple point location is quite far from the wall as compared to experiment. Therefore, the reflected expansion effect is not felt in computed wall pressure at x = 11.5 cm in Fig. 5a. The presence of the separation bubble causes a deviation of the streamlines and in consequence, the formation of the separation shock, followed by a nearly constant pressure region (i.e. the plateau) in correspondence with the recirculation boundary layer region. The heat transfer reaches a maximum at x = 11.5 cm in Fig. 5b due to the greater boundary layer compression below the T. Here, it is observed that the skin friction C_f decreases before S due to the thickening of the boundary layer up to -10 cm. The skin friction evidently becomes negative as the velocity gradients become negative owing to reversing flow. The skin friction and heat transfer rapidly increase downstream of reattachment due to the flow recompression and have a peak past reattachment at the location where boundary layer thickness is minimum.

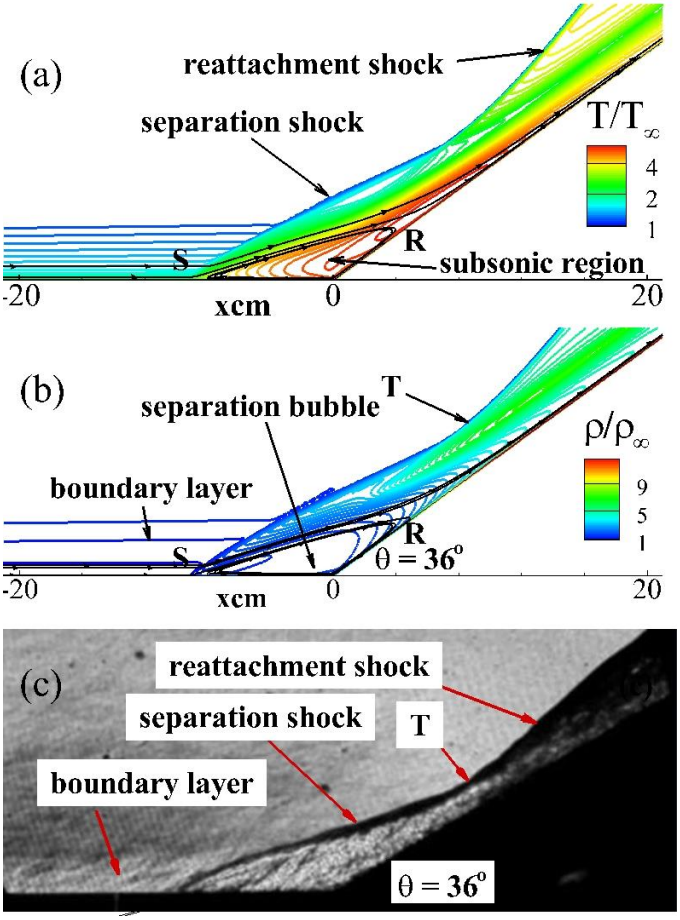

Figure 4: The computed flow field in terms of (a) temperature and (b) density contours using modified limiter k-ω model [17], compared with the experimental data [27].

DOI: 10.13009/EUCASS2019-938

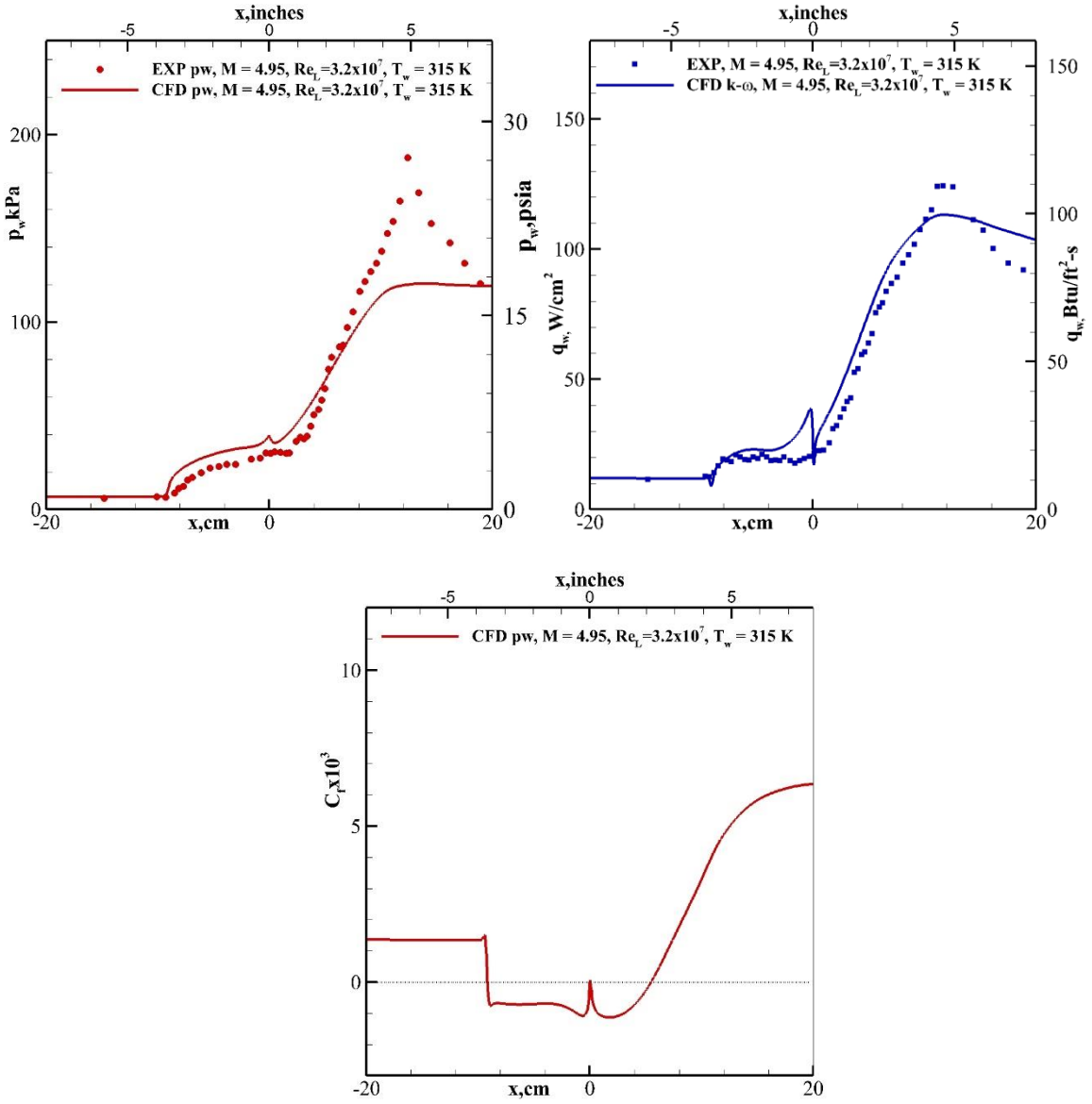

Figure 5: Comparison of computed (a) wall pressure and (b) heat flux compared using standard k-ω model [16] and modified k-ω model [17] with different limiter values compared with the experimental data [28].

Standard and modified k-ω model results

The standard two-equation k-ω model was designed for incompressible flows [16]. Therefore, it results in high values of turbulence across shock waves and at stagnation points in high-speed flows[7]. To avoid nonphysical build-up of turbulence across shock waves, a production term limiter designed by Menter et al. [17] is used in the simulations and is given by

$$P_k = (P_{k,k\text{-}\omega}, K\rho\omega) \qquad \text{Eq. (1)}$$

The production limiter was used by researchers in 3D and 2D SWTBLI flows both at supersonic and hypersonic Mach numbers to improve the results in the interaction region [29],[7],[6]. Figure 6 shows a comparison of computed wall pressure, heat flux, and skin friction and Fig. 7 shows eddy viscosity levels using standard two-equation k-ω model [16] and its modified form with limiter [17].

DOI: 10.13009/EUCASS2019-938

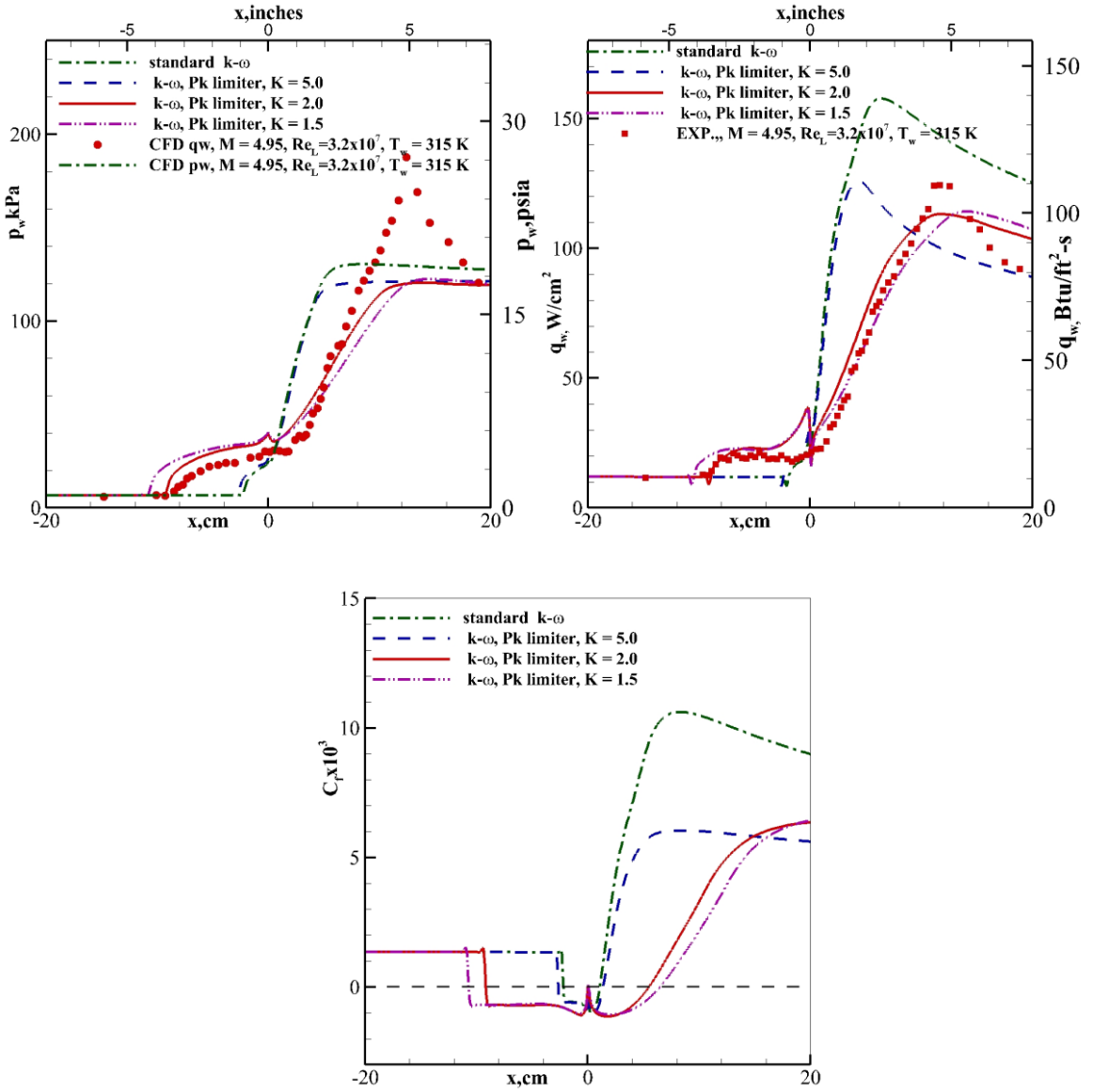

Figure 6: Comparison of computed (a) wall pressure and (b) heat flux and (c) skin friction using standard k-ω model [16] and modified limiter k-ω model [17] with different limiter values, K compared with the experiments [28].

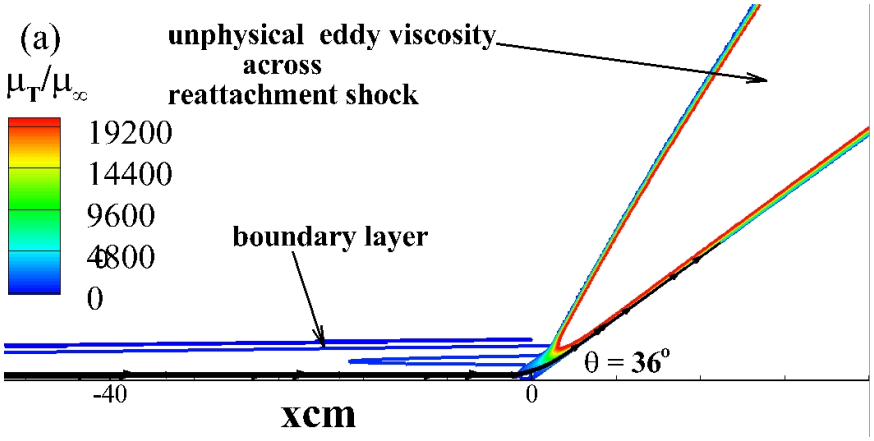

DOI: 10.13009/EUCASS2019-938

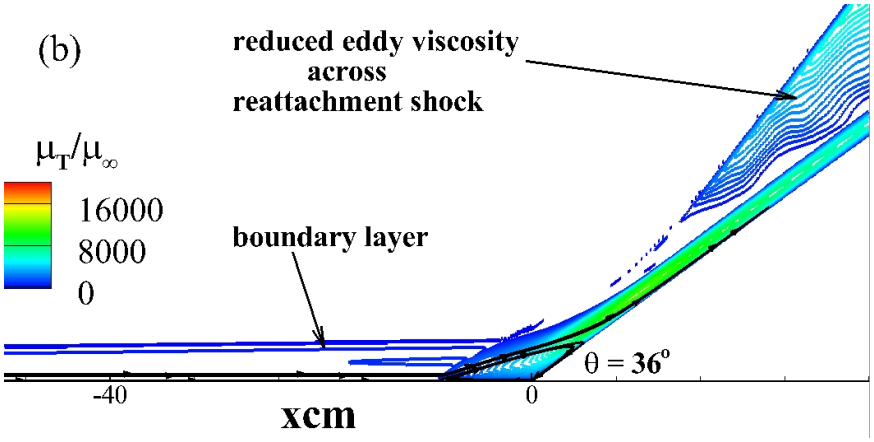

Figure 7: Comparison of computed eddy viscosity (a) standard k-ω model [16] and (b) modified k-ω model [17] with limiter with K = 2.0.

Fig.6a shows that standard k-ω turbulence model predicts an initial pressure rise location at x = -2.3 cm. It does not catch up with the pressure rise in the plateau region between -8.5 cm to 1.76 cm and reattachment region at 12.6 cm in comparison to the experimental data. The heat flux is over predicted in the upstream region at x = 6.4 cm when compared to the experiments and these peak values are attributed to the higher values of P_k by the standard model. A small separation bubble of 3.2 cm is observed in Fig.6c.

Figure 6 shows the skin friction sensitivity to the production energy term limiter K as given in Eq.1 on SBLI region. It is observed that as the value of K increases the production of turbulent kinetic energy reduces across shock wave and pushes the separation point location upstream w.r.t. to the cylinder-flare corner. The modified limiter of the production energy term in the k-ω model predicts initial pressure location close to the experimental value with K = 2.0 as given in Eq.1 (see Fig.6a) in comparison to the standard model. The value of K = 5 matches with that of the K value in the standard of the k-ω model when analyzing the wall properties except of course in the reattachment region and beyond. The heat flux variation in Fig. 6b shows a good match with the experiment in the pressure plateau and reattachment regions. The separation bubble size increases with the lower values of K in Fig. 6c. A separation bubble size of 14.5 cm is observed with a value of K = 2.0.

It is observed that the standard k-ω gives unphysical rise of turbulence levels across bow sock in case of blunt hypersonic bodies and across shocks in SBLI cases especially in the inviscid regions [30],[31]. Therefore, the production limiter is used extensively to stop the unphysical rise of turbulence levels across shocks in hypersonic flows[30],[31]. This unphysical increase of the turbulent quantities induced by shock wave with the application of standard two-equation k-ω model [16] (the model uses Pk without limiter) is shown in Fig.7 in terms of eddy viscosity normalized with free stream absolute viscosity value It is observed that the increase in the magnitude of eddy viscosity across a shock wave is reduced in comparison to the standard model in Fig. 7. It is observed that the Pk with limiter reduces but cannot eliminate the unphysical increase of the turbulent quantities across a shock wave completely. A shock unsteadiness model removes this unphysical turbulence levels across shock waves in the inviscid regions of an oblique shock boundary layer interaction flows at Mach 5 [32]. The shock unsteadiness model will be applied in our future studies for the current test case.

4. Three-dimensional numerical simulations

Numerical method

The CFD code used in this work makes use of the strong conservation form of the Navier-Strokes equations and for a solution, purposes adopt an implicit approximate factorization scheme due to Beam and Warming [12]. Local time linearization is applied to the non-linear terms and a three-station backward implicit time differencing and a second order finite difference approximation is applied to all spatial derivatives in the code. The spatial derivative terms are approximated with second-order central differences. Explicit and implicit artificial dissipation terms are added to achieve non-linear stability. For the present calculations, the solver was run in a steady state mode. It can treat upstream free boundary conditions and an extrapolation method to handle far downstream flow conditions. Euler/Slip and no-slip viscous wall conditions can be invoked automatically. Second and fourth order dissipation coefficients having values of 0.25 and 0.64 were implemented in the equations to help towards convergence. A spatially variable time step is used to accelerate convergence for steady-state calculation. Owing to the high Mach number nature of the

DOI: 10.13009/EUCASS2019-938

present investigation an appropriate correction [33] to γ was implemented in the code. The k-ω turbulence due to Wilcox [16] is used for the viscous closure. The cylindrical slice representing the computational domain was equipped with a no-slip isothermal boundary condition at the surface with a far-field boundary condition at the opposite free edge. The incoming flow was set at free stream conditions and far downstream was designated as the far extrapolation boundary condition. The two azimuthal boundaries in the cylindrical directions were equipped with a reflection plane/Euler boundary condition.

Grid topology

During the present investigation, several grid strategies were adapted to capture the shock effectively and resolve the strong shock boundary layer interaction which occurs in the junction region. The grid was produced by first creating a normal 2D plane representing a vertical section, which was subsequently rotated in azimuthal direction through 5 steps of π/360 radian each. Starting from a coarse mesh which measured 169 x 50 x 5 to an extremely dense mesh of dimensions 600 x 500 x 5 were studied in turn to see which topology best suited for efficient and accurate resolution. It was finally decided to run a mesh of dimensions 240 x 100 x 5 as it provided reasonably fast turn-around times along with the desired accuracy. The mesh used in this study is shown in Fig. 8 and the computed wall pressure is shown in Fig. 9. In the first part of the investigation, the mesh suitability was studied at length. As mentioned above, a number of grids of varying dimensions were run at flow conditions taken from Holden [28] with Mach number M = 4.95 unit Reynolds number/m 1.2 x 107.

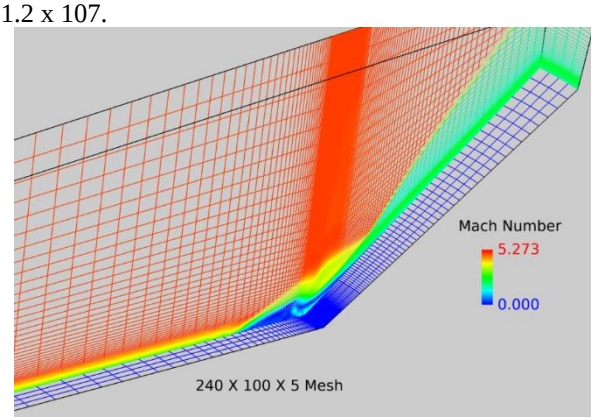

Figure 8. 3D Mesh.

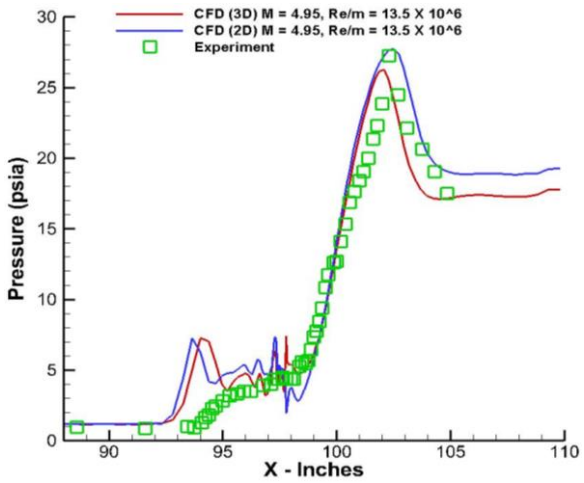

Figure 9: Pressure distribution.

DOI: 10.13009/EUCASS2019-938

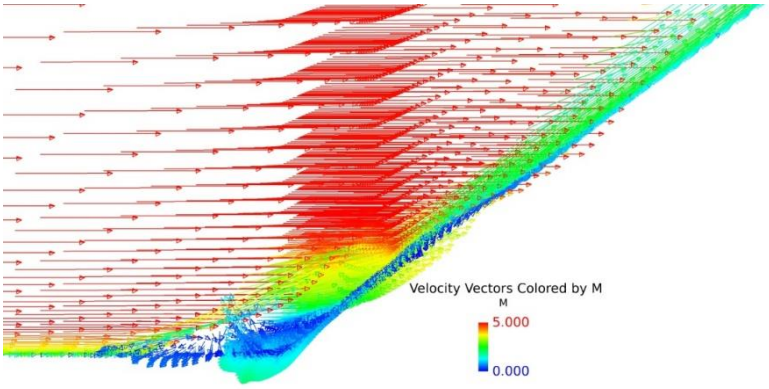

Fig 10. Velocity vectors colored by Mach Number from a 3D simulation.

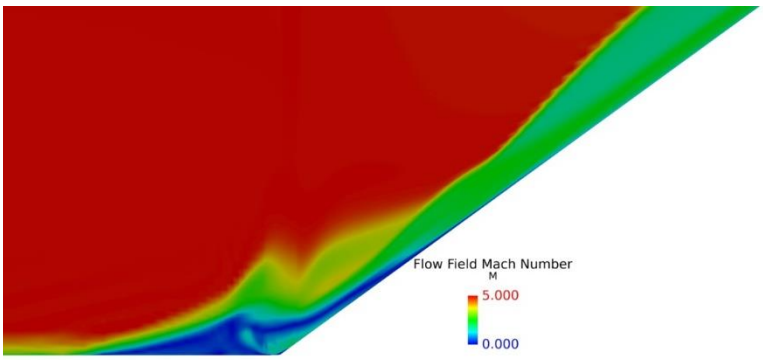

Figure 11: Mach Number based flow field from a 3D.

Results and discussions

Fig.9 shows the surface pressure distribution on the Large Cylinder Cone configuration from different 3D and 2D calculations at free stream conditions M = 4.95, Re/m = 1.2 x 10^7. Surprisingly the 2D computation can pick up the peak pressure more accurately than the corresponding 3D computation. Otherwise, both types of solutions produced similar behaviour elsewhere. Both solutions show a larger junction region stagnated flow than indicated by the experiment. The stagnated flow in the junction region is further explored in terms of the velocity vectors coloured by Mach numbers. The reversing flow appears to forcibly separate the flow producing a lengthy stagnation region which results in a bubble as observed in Fig 10. The corresponding Mach number-based flow field from the 3D computation is shown in Fig. 11. It is clear from the flow field examination in the junction region that there is a strong interplay between the shock emanating from the junction and the boundary layer. This leads to physical unsteadiness in the junction region which of course would not be resolved using steady-state computations. In fact, the reversing flow produces a strong vortex in the corner which straddles both horizontal and inclined surface. This vortex would oscillate too and for as it tries to adjust with the shock. A layer of the blue region stretching from the horizontal surface is forced upwards as it works its way past the faster-reverting flow descending from the conical surface before it attaches on to the surface of the incline. More energetic flow is thus trapped inside this slower layer of the flow. As observed in the pressure distribution shown in Fig.9, the unsteady pressures are easily picked up by both the computation and the experiment in the junction region.

It is obvious that the unsteady flow brought about by the bubble in the junction region has global implications for the entire flow field. A Reynolds stress averaged solver equipped with a turbulence model calibrated and validated under steady flow condition tries to enforce unsteadiness on the flow field which is consistently resisted by the unsteady flow field. Towards this end then, a pressure distribution trace produced in the junction at one converged solution iteration will differ with the next one. The solution thus is numerically unstable and even under converged conditions continues to oscillate. It should be mentioned that the solution converged well beyond two orders of magnitude in L2 based conservation of variables. The history is shown in Fig. 12. The solutions started with a sharp increase in residuals before proceeding towards its downwards trend. The sharp spikes indicate the spots where the time step was adjusted for faster convergence.

DOI: 10.13009/EUCASS2019-938

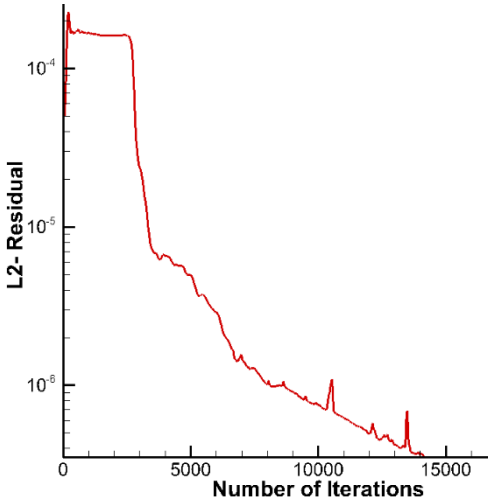

Figure 12: Convergence history.

The heat transfer calculations were also obtained from the present computations from this 240 x 100 x 5 mesh. The comparison is appropriately shown in Fig.13. Except for the junction region where the computed heat transfer results are notably higher than the measurement, the simulations follow the experiment quite closely. The computed results for both 2D and 3D simulations continue to show large oscillations in the junction region which is indicative of the highly unsteady flow in this region. The peak values for the 2D simulation are under-predicted compared to the experiment. The strong vortex produced in simulations gives rise to accentuated heat transfer rates in the junction region.

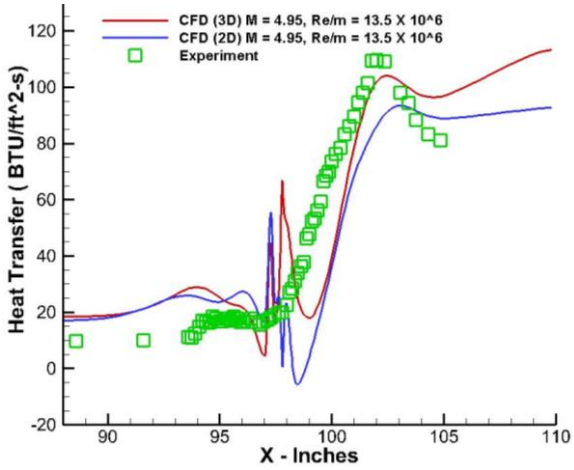

Figure 13. Heat transfer rate comparisons.

The skin friction for the above flow conditions M = 4.95 and unit Reynolds number/m 1.2 x 10^7 is shown in Fig.14 The extent of the reversing flow and the bubble region is equally captured both by 2D and 3D computation. or the higher Mach number case is far more confined as is the magnitude of the skin friction oscillations.

DOI: 10.13009/EUCASS2019-938

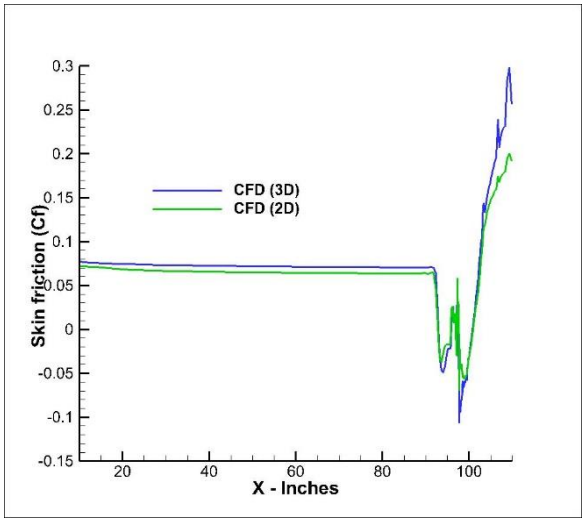

Figure 14**:** Skin Friction, M = 4.95 and Reynolds number/m 1.2 x 10^7

5. Conclusions

With the careful and selective distribution of grid points on the strategic location of the large cylinder Cone configuration, it is possible to compute pressure and heat transfer rate trends for both 2D and 3D configurations. The computed results were close to precise pressure peaks and their locations. The stagnated junction flow is highly unsteady owing to the strong interaction between the strong shock produced at the junction and viscous boundary layer. A steady computation forces a time-averaged steadiness upon an otherwise unsteady flow giving the solution which is close to the reality but lacks the precise accuracy which could be obtained in a purely unsteady solution. Convergence problems are encountered when the numerical instability in the junction region becomes unwieldy by algorithms written for steady state flows. It was learned that using the production energy term limiter K leads to the successful simulation of hypersonic flow past 2D configuration which represents a complex 3D geometry comprising a large long cylinder with a 36° flared cone at the downstream end. It was equally encouraging to see that when the same geometry is a run in a 3D mode with an appropriate Mach number correction to γ even with standard k-ω turbulence model gave satisfactory results. Even 2D simulations seemed to closely mimic their 3D counterparts.

Acknowledgments

The authors would like to thank the Aziz High-Performance Computing (HPC) facility to perform numerical simulations. Dr. Amjad would like to thank Professor K. Sinha from IIT Bombay, Department of Aerospace Engineering for his kind help.

References

[1] J. G. Marvin, J. L. Brown, and P. A. Gnoffo, “Experimental Database with Baseline CFD Solutions : 2-D and Axisymmetric Hypersonic Shock-Wave / Turbulent-Boundary-Layer Interactions,” *NASA Tech. Memo.*, no. November 2013, 2013.

[2] P. G. Huang and T. J. Coakley, “hypersonic flows using compressible b functions The compressible law of the,” 1993.

[3] D. Knight and G. Degrez, “Shock Wave Boundary Layer Interactions in High Mach Number Flows A Critical Survey of Current Numerical Prediction Capabilities,” *Agard Advis. Rep. Agard Ar*, vol. 2, p. 35, 1998.

[4] D. Knight, H. Yan, A. G. Panaras, and A. Zheltovodov, “Advances in CFD prediction of shock wave turbulent boundary layer interactions,” *Prog. Aerosp. Sci.*, vol. 39, no. 2–3, pp. 121–184, 2003.

[5] C. J. Roy and F. G. Blottner, “Review and assessment of turbulence models for hypersonic flows,” *Prog. Aerosp. Sci.*, vol. 42, no. 7–8, pp. 469–530, 2007.

[6] D. V. Gaitonde, “Progress in shock wave/boundary layer interactions,” *Prog. Aerosp. Sci.*, vol. 72, pp. 80–99, 2015.

[7] Z. Zhang, Z. Gao, C. Jiang, and C. H. Lee, “A RANS model correction on unphysical over-prediction of turbulent quantities across shock wave,” *Int. J. Heat Mass Transf.*, vol. 106, pp. 1107–1119, 2017.

[8] P. A. Gnoffo, “CFD validation studies for hypersonic flow prediction,” 2001.

[9] G. Candler, I. Nompelis, and M.-C. Druguet, “Navier-Stokes predictions of hypersonic double-cone and

DOI: 10.13009/EUCASS2019-938

cylinder-flare flow fields," no. c, 2013.
[10] I. Nompelis and G. V. Candler, "US3D Predictions of Double-Cone and Hollow Cylinder-Flare Flows at High-Enthalpy (Invited)," no. June, pp. 1–21, 2014.
[11] R. W. MacCormack and G. V Candler, "The solution of the Navier-Stokes equations using Gauss-Seidel line relaxation," *Comput. Fluids*, vol. 17, no. 1, pp. 135–150, 1989.
[12] R. M. Beam and R. Warming, "An implicit factored scheme for the compressible Navier-Stokes equations," *AIAA J.*, vol. 16, no. 4, pp. 393–402, 1978.
[13] M. S. Holden and M. Maclean, "Measurements in Regions of Shock Wave / Turbulent Boundary Layer Interaction on Double Cone and Hollow," no. June, 2014.
[14] D. C. Wilcox, *Turbulence modeling for CFD*, Third. DCW industries La Canada, CA, 2006.
[15] K. Sinha and G. Candler, "Convergence improvement of two-equation turbulence model calculations," in *In 29th AIAA Fluid Dynamics Conference, Albuquerque, NM*, 1998.
[16] D. C. Wilcox, "Reassessment of the scale-determining equation for advanced turbulence models," *AIAA J.*, vol. 26, no. 11, pp. 1299–1310, 1988.
[17] F. R. Menter, "Review of the shear-stress transport turbulence model experience from an industrial perspective," *Int. J. Comut. Fluid Dyn.*, vol. 23, no. 4, pp. 305–316, 2009.
[18] M. J. Wright, D. Bose, and G. V. Candler, "Data-Parallel Line Relaxation Method for the Navier-Stokes Equations," *AIAA J.*, vol. 36, no. 9, pp. 1603–1609, 1998.
[19] F. R. Menter, "Two-equation eddy-viscosity turbulence models for engineering applications," *AIAA J.*, vol. 32, no. 8, pp. 1598–1605, 1994.
[20] K. Sinha, K. Mahesh, and G. V. Candler, "Modeling the Effect of Shock Unsteadiness in Shock/ Turbulent Boundary-Layer Interactions," *AIAA J.*, vol. 43, no. 3, pp. 586–594, 2008.
[21] A. A. Pasha and K. Sinha, "Simulation of Hypersonic Shock/Turbulent Boundary-Layer Interactions Using Shock-Unsteadiness Model," *J. Propuls. Power*, vol. 28, no. 1, pp. 46–60, 2012.
[22] P. Raje and K. Sinha, "A physically consistent and numerically robust k-ε model for computing turbulent flows with shock waves," *Comput. Fluids*, vol. 136, pp. 35–47, 2016.
[23] A. A. Pasha, K. A. Juhany, and M. Khalid, "Numerical prediction of shock/boundary-layer interactions at high Mach numbers using a modified Spalart-Allmaras model," *Eng. Appl. Comput. Fluid Mech.*, vol. 12, no. 1, pp. 459–472, Jan. 2018.
[24] A. A. Pasha, "Study of Parameters Affecting Separation Bubble Size in High Speed Flows using k-ωTurbulence Model," *J. Appl. Comput. Mech.*, vol. 4, no. 2, pp. 95–104, 2018.
[25] A. A. Pasha, "Three-Dimensional Modeling Shock-Wave Interaction with a Fin at Mach 5," *Arab. J. Sci. Eng.*, Mar. 2018.
[26] A. A. Pasha and K. A. Juhany, "Computation of Hypersonic Flows on Compression Corner using modified k-w model," in *HiSST : International Conference on High-Speed Vehicle Science Technology*, 2018, no. November, pp. 1–18.
[27] M. S. Holden, T. P. Wadhams, and M. Maclean, "Measurements in Regions of Shock Wave / Turbulent Boundary Layer Interaction From Mach 4 To 10 for Open and ' Blind ' Code Evaluation / Validation Review of Recent Comparisons Between Predictions and Experiments in Hypersonic Turbulent Interactions (Open," no. March, pp. 1–25, 2013.
[28] M. S. Holden, "Measurements in laminar regions of shock/shock and shock/boundary layer interaction over cylindrical leading edges, cone/cone and hollow cylinder flare configurations for DSMC/Navier-Stokes code validation," *AIP Conf. Proc.*, vol. 585, pp. 699–706, 2001.
[29] D. V Gaitonde, M. R. Visbal, and J. S. Shang, "Sidewall Interaction in an Asymmetric Simulated Scramjet Inlet Con guration," vol. 17, no. 3, 2001.
[30] P. Gnoffo, B. Hollis, C. O. Johnston, J. L. Brown, D. K. Prabhu, and D. Bose, "Uncertainty Assessment of Hypersonic Aerothermodynamics Prediction Capability," *J. Spacecr. Rockets*, vol. 50, no. 1, pp. 12–18, 2013.
[31] J. L. Brown, "Hypersonic Shock Wave Impingement on Turbulent Boundary Layers: Computational Analysis and Uncertainty," *J. Spacecr. Rockets*, vol. 50, no. 1, pp. 96–123, 2013.
[32] A. A. Pasha and K. Sinha, "Shock-unsteadiness model applied to oblique shock wave/turbulent boundary-layer interaction," *Int. J. Comut. Fluid Dyn.*, 2008.
[33] M. Khalid and K. A. Juhany, "Heat alleviation studies on hypersonic re-entry vehicles," *Aeronaut. J.*, vol. 122, no. 1257, pp. 1673–1696, 2018.